

## Phase diagram and physical properties of $\text{NaFe}_{1-x}\text{Cu}_x\text{As}$ single crystals

A. F. Wang, J. J. Lin, P. Cheng, G. J. Ye, F. Chen, J. Q. Ma, X. F. Lu, B. Lei, X. G. Luo, and X. H. Chen\*

Hefei National Laboratory for Physical Science at Microscale and Department of Physics, University of Science and Technology of China, Hefei, Anhui 230026, People's Republic of China

(Received 23 July 2013; revised manuscript received 8 September 2013; published 25 September 2013)

A series of high-quality  $\text{NaFe}_{1-x}\text{Cu}_x\text{As}$  single crystals have been grown with the self-flux technique, which were systematically characterized via structural, transport, thermodynamic, and high-pressure measurements. Both the structural and magnetic transitions are suppressed by Cu doping, and bulk superconductivity is induced by Cu doping. The superconducting transition temperature ( $T_c$ ) is initially enhanced from 9.6 to 11.5 K by Cu doping, and then suppressed with further doping. A phase diagram similar to  $\text{NaFe}_{1-x}\text{Co}_x\text{As}$  is obtained except that semiconducting instead of metallic behavior is observed in the extremely overdoped samples.  $T_c$ s of underdoped, optimally doped, and overdoped samples are all notably enhanced by applying pressure. Although a universal maximum transition temperature ( $T_c^{\text{max}}$ ) of about 31 K under external pressure is observed in underdoped and optimally doped  $\text{NaFe}_{1-x}\text{Co}_x\text{As}$ ,  $T_c^{\text{max}}$  of  $\text{NaFe}_{1-x}\text{Cu}_x\text{As}$  is monotonically suppressed by Cu doping, suggesting that impurity potential of Cu is stronger than that of Co in  $\text{NaFeAs}$ . The comparison between Cu and Co doping effect in  $\text{NaFeAs}$  indicates that Cu serves as an effective electron dopant with strong impurity potential, but part of the doped electrons are localized and do not fill the energy bands as predicted by the rigid-band model.

DOI: [10.1103/PhysRevB.88.094516](https://doi.org/10.1103/PhysRevB.88.094516)

PACS number(s): 74.70.Xa, 74.25.F-, 74.62.Dh

### I. INTRODUCTION

The discovery of iron-based superconductors gives another opportunity to study the physics of high-temperature superconductivity besides the cuprates.<sup>1-3</sup> The parent compounds of iron-based superconductors are antiferromagnetic semimetals, and superconductivity can be induced by hole and electron doping or applying pressure. For example, superconductivity was induced in  $\text{BaFe}_2\text{As}_2$  by the doping of Co, Ni, and Cu.<sup>4,5</sup> In the case of Co and Ni doping, the doped electron numbers predicted by the rigid-band model are  $x$  and  $2x$ , respectively. The study on the phase diagram of  $\text{Ba}(\text{Fe}_{1-x}\text{Co}_x)_2\text{As}_2$  and  $\text{Ba}(\text{Fe}_{1-x}\text{Ni}_x)_2\text{As}_2$  with angle-resolved photoemission spectroscopy (ARPES) indicates that the doped electron number roughly follows the rigid-band model.<sup>6</sup> Therefore, it is natural to expect that superconductivity could be induced by Cu doping and the doped electron number is  $3x$ . However, superconductivity was observed in a very narrow range of doping in  $\text{Ba}(\text{Fe}_{1-x}\text{Cu}_x)_2\text{As}_2$ ,<sup>5</sup> and no superconductivity was observed in  $\text{Sr}(\text{Fe}_{1-x}\text{Cu}_x)_2\text{As}_2$ .<sup>7</sup>

Although the doping effect of Co and Ni is clear now, the role of Cu doping is still under debate. X-ray photoelectron spectroscopy (XPS) and x-ray absorption (XAS) measurements show that Cu  $3d$  states locate at the bottom of the valence band in a localized  $3d^{10}$  shell, so that the formal valence state of Cu is  $+1$  and the substitution of  $\text{Fe}^{2+}$  by  $\text{Cu}^{1+}$  results in hole doping.<sup>7-9</sup> The theoretical and experimental studies on  $\text{SrCu}_2\text{As}_2$ , the end member of the  $\text{Sr}(\text{Fe}_{1-x}\text{Cu}_x)_2\text{As}_2$  series, indicate that it is an  $sp$ -band metal with hole-type carriers dominant, and Cu in the nonmagnetic  $3d^{10}$  electronic configuration corresponds to the valence state  $\text{Cu}^{1+}$ ,<sup>7,10,11</sup> which further supports the result of XPS and XAS. In addition, the doping effect of Cu is similar to that of Mn, which is also considered as hole doping and no superconductivity has been found.<sup>12</sup> On the contrary, however, electron doping by Cu was proved by ARPES in  $\text{Ba}(\text{Fe}_{1-x}\text{Cu}_x)_2\text{As}_2$ ,<sup>6</sup> and further confirmed by Hall measurement on  $\text{Ba}_{0.6}\text{K}_{0.4}(\text{Fe}_{1-x}\text{Cu}_x)_2\text{As}_2$ .<sup>13</sup> A superconducting dome similar to that of  $\text{Ba}(\text{Fe}_{1-x}\text{Co}_x)_2\text{As}_2$  was

observed in the phase diagram of  $\text{Ba}(\text{Fe}_{1-x-y}\text{Co}_x\text{Cu}_y)_2\text{As}_2$  ( $x \sim 0.022$  and  $x \sim 0.047$ ),<sup>5</sup> indicating the similar doping effect between Co and Cu, and further suggesting that it is the electron carriers that are induced by Cu doping. To reconcile this controversial situation, it is of great interest to further investigate the Cu doping effect in other families of iron-pnictide superconductors.

Besides  $\text{BaFe}_2\text{As}_2$ , high-quality  $\text{NaFeAs}$  single crystals are also available now, which turn out to be suitable for studying the Cu doping effect.  $\text{NaFeAs}$  is regarded as a filamentary superconductor. By substituting Co or Ni on Fe sites, bulk superconductivity was obtained.<sup>14,15</sup> The Ni doping doubles the amount of electron doping by Co,<sup>14</sup> which follows the rigid-band model. It has been reported that  $T_c$  of the analogous compound  $\text{LiFe}_{1-x}\text{Cu}_x\text{As}$  is suppressed linearly by Cu doping.<sup>16</sup> Hence, we study the role of Cu doping in  $\text{NaFe}_{1-x}\text{Cu}_x\text{As}$ , and compare it with the effect of Cu doping in  $\text{BaFe}_2\text{As}_2$  and  $\text{LiFeAs}$ . In this paper, we report the study on the physical properties and phase diagram of  $\text{NaFe}_{1-x}\text{Cu}_x\text{As}$  by performing x-ray diffraction (XRD), resistivity, magnetic-susceptibility, Hall, specific-heat, and high-pressure measurements. A phase diagram similar to  $\text{NaFe}_{1-x}\text{Co}_x\text{As}$  is established. The comparison of the physical properties and phase diagrams between  $\text{NaFe}_{1-x}\text{Cu}_x\text{As}$  and  $\text{NaFe}_{1-x}\text{Co}_x\text{As}$  clearly indicates that Cu doping is electron doping and the electron number deviates from the expected  $3x$ . The deviation can be explained that part of the doped electrons fill the impurity band which is located deep below the Fermi level ( $E_F$ ) and do not fill the energy bands as predicted by the rigid-band model.<sup>6,9</sup>

### II. EXPERIMENTAL DETAILS

A series of  $\text{NaFe}_{1-x}\text{Cu}_x\text{As}$  single crystals were grown by adopting the NaAs flux method. The growth procedure resembles that of  $\text{NaFe}_{1-x}\text{Co}_x\text{As}$ .<sup>15</sup> The NaAs precursor was first prepared by reacting the Na chunks and As powder in an evacuated quartz tube at 200 °C for 10 hours. The powders

of NaAs, Fe, and Co were mixed together according to the ratio NaAs : Fe : Cu = 4 : 1 -  $x$  :  $x$ . Then, the mixture was placed into an alumina crucible and sealed inside an iron crucible under Ar atmosphere. The sealed iron crucible was slowly heated to 950 °C in a tube furnace filled with Ar gas. After being kept at 950 °C for 10 h, the sample was cooled to 600 °C at a rate of 3 °C/h to grow single crystals. The shiny crystal can be easily cleaved mechanically from the melt, and the dimensions of the single crystal can go up to  $15 \times 10 \times 0.3 \text{ mm}^3$ . All the operation must be carried out in glove box in which high pure argon atmosphere is filled.

It is well known that NaFeAs single crystals are air and moisture sensitive. Similar to the electron doping effect, both structural and SDW transitions are suppressed and  $T_c$  is enhanced by exposing NaFeAs in the air.<sup>17</sup> In order to obtain intrinsic physical properties, great attention should be paid to handle NaFe<sub>1-x</sub>Cu<sub>x</sub>As single crystals. Samples must be stored and transported in sealed containers filled with an inert gas. If we must prepare samples for resistivity or other measurements in the air, it is necessary to do the experiment in a dry room with the temperature lower than 20 °C. It is also noteworthy that NaAs flux is highly air sensitive, which should be removed from the surface of the crystals before being exposed in the air. As a result, no obvious degrading effect is observed within an hour.<sup>18</sup>

XRD was performed on a Smartlab-9 diffractometer (Rikagu) from 10° to 70°, with a scanning rate of 6° per minute. The actual chemical composition of the single crystal was determined by energy-dispersive x-ray spectroscopy (EDX) mounted on the field emission scanning electronic microscope (FESEM), Sirion 200. The Cu content  $x$  hereafter is the actual composition determined by EDX. The resistivity measurements were carried out by using the PPMS-9T (Quantum Design), and resistivity down to 50 mK was measured in a dilution refrigerator on PPMS. Electrical contacts used in resistivity measurements were made to the samples using silver paste (Dupont 4929N) to attach Pt wires in a standard four-probe configuration, and the contact resistance is less than 100 mΩ at room temperature. Specific-heat data were collected in a PPMS using the thermal relaxation technique. The magnetic susceptibility was measured using a vibrating sample magnetometer (VSM) (Quantum Design). The Hall coefficient was measured on PPMS with the four-terminal ac technique by switching the polarity of the magnetic field  $H//c$  to remove any magnetoresistive components due to the misalignment of the voltage contacts.<sup>19</sup> The pressure was generated in a Teflon cup filled with Daphne oil 7373, which was inserted into a Be-Cu pressure cell, and the pressure applied in the resistivity measurement was determined by the shift of superconducting transition temperature of pure Sn.<sup>20</sup>

### III. RESULTS

#### A. X-ray diffraction

Figure 1(a) shows the selected single-crystalline XRD patterns for the NaFe<sub>1-x</sub>Cu<sub>x</sub>As single crystals. Only (00 $l$ ) reflections can be recognized, indicating that the crystals are well orientated along the  $c$  axis. The lattice parameter  $c$  is estimated from the (00 $l$ ), and the evolution of  $c$  of

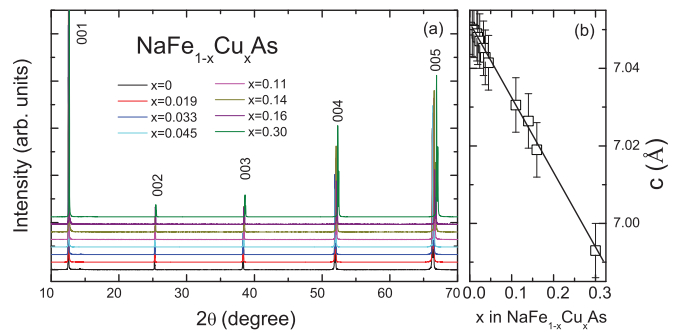


FIG. 1. (Color online) (a) Selected XRD patterns for the NaFe<sub>1-x</sub>Cu<sub>x</sub>As single crystals. (b) Doping dependence of the  $c$ -axis parameter.

all the single crystals with the doping level is shown in Fig. 1(b).  $c$  decreases with increasing doping concentration, which roughly obeys Vegard's law. Comparing with undoped NaFeAs, the amplitude of the lattice parameter change is about 0.8% with Cu doping concentration up to 0.30, a little smaller than that of Co-doped NaFeAs with the same doping level.<sup>14,15</sup>

#### B. Electrical resistivity

The temperature dependence of in-plane electrical resistivity for NaFe<sub>1-x</sub>Cu<sub>x</sub>As single crystals is shown in Fig. 2. To make the graphs easier to read, the data are grouped into three sets. The resistivity of NaFe<sub>1-x</sub>Cu<sub>x</sub>As at room temperature is about 0.4–1.7 mΩ cm, similar to that of NaFe<sub>1-x</sub>Co<sub>x</sub>As.<sup>15,21</sup> Comparing to the change of absolute resistivity caused by the doping effect, the error bar of our data is relatively large, which is mainly coming from the uncertainty of the geometric factor. As a result, we cannot observe a completely systematic evolution of the room-temperature resistivity within the whole doping range. The superconducting transitions for most of

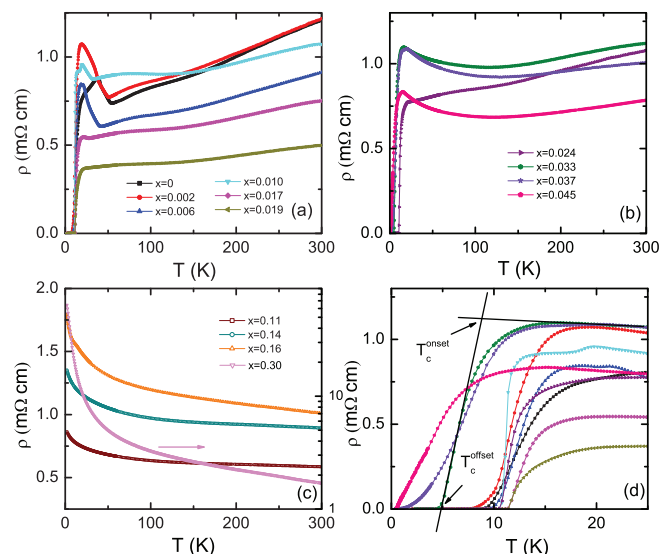


FIG. 2. (Color online) (a)–(c) Temperature dependence of in-plane resistivity for NaFe<sub>1-x</sub>Cu<sub>x</sub>As single crystals. (d) Enlargement of the low-temperature resistivity in panels (a) and (b). The criteria used to determine the onset and offset temperature for the superconducting transitions are also shown in (d).

the samples are quite broad and the onset is very round, so we define  $T_c^{\text{offset}}$  as  $T_c$ , as shown in Fig. 2(d).  $T_c$  stands for  $T_c^{\text{offset}}$  for convenience hereafter. The kinks associated with the structural/spin density wave (SDW) transition can be clearly recognized in the low-temperature resistivity of underdoped crystals.<sup>22</sup> The criteria used to define the structural and SDW transitions are shown in Fig. 7.

The structural and SDW transitions are progressively suppressed with increasing Cu concentration, similar to that of NaFe<sub>1-x</sub>Co<sub>x</sub>As.  $T_c$  increases slightly with Cu doping in the underdoped region. The maximum  $T_c$  about 11.5 K is reached at  $x = 0.019$ , but the amplitude of  $T_c$  enhancement (2 K) is much smaller than that in Co-doped NaFeAs (10 K).  $T_c$  decreases quickly with further doping, and no trace of superconducting transition is observed in crystals with doping concentration higher than 0.045. The metal-insulator transition is observed in the crystals with  $x \geq 0.033$ . Ultimately, semiconducting behavior in the whole temperature range is observed in the extremely overdoped crystals, which is quite different from the metallic behavior in extremely overdoped NaFe<sub>1-x</sub>Co<sub>x</sub>As.<sup>15</sup> A weak semiconducting behavior is also observed in Ba(Fe<sub>1-x</sub>Cu<sub>x</sub>)<sub>2</sub>As<sub>2</sub> and Sr(Fe<sub>1-x</sub>Cu<sub>x</sub>)<sub>2</sub>As<sub>2</sub>.<sup>5,7</sup> In addition, when ~4% Fe was substituted by Cu, a metal-insulator transition was observed in Fe<sub>1.01-x</sub>Cu<sub>x</sub>Se.<sup>23,24</sup> It was reported that the insulator phase of Fe<sub>1.01-x</sub>Cu<sub>x</sub>Se is an Anderson localized system arising from disorder rather than a conventional semiconductor.<sup>25</sup> Whether the semiconductor-like behavior in NaFe<sub>1-x</sub>Cu<sub>x</sub>As and Fe<sub>1.01-x</sub>Cu<sub>x</sub>Se have common origin needs further investigation.

### C. Magnetic susceptibility

Figure 3 shows the zero-field-cooling (ZFC) magnetic susceptibility taken at 10 Oe with  $H$  perpendicular to the  $c$  axis for the superconducting NaFe<sub>1-x</sub>Cu<sub>x</sub>As single crystals. We define  $T_c^X$  as the temperature at which the susceptibility starts to drop. As reported previously, a tiny diamagnetic signal was observed below 9 K in undoped NaFeAs.<sup>15</sup> With Cu doping, the superconducting shielding fraction rises rapidly. Bulk superconductivity with large shielding fraction is observed in the composition with a range of 0.006 ~ 0.024, indicating that Cu doping is beneficial to the superconductivity of NaFeAs.  $T_c$ s inferred from the diamagnetic signal are consistent with those determined by resistivity measurements. As shown in

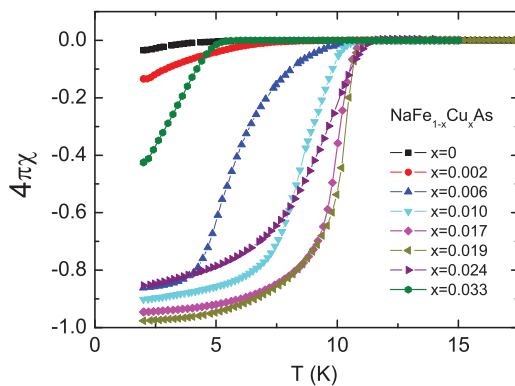


FIG. 3. (Color online) Temperature-dependent magnetic susceptibility for NaFe<sub>1-x</sub>Cu<sub>x</sub>As with magnetic field 10 Oe.

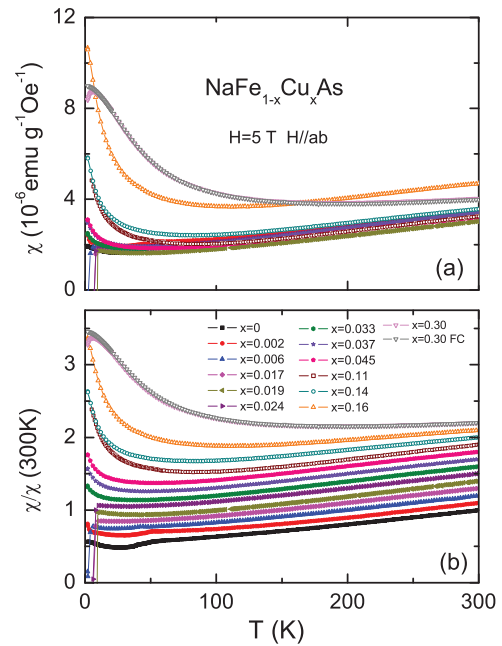


FIG. 4. (Color online) (a) Temperature dependence of normal-state magnetic susceptibility for NaFe<sub>1-x</sub>Cu<sub>x</sub>As under a magnetic field of 5 T. (b) Temperature dependence of the normalized magnetic susceptibility, which is shifted upward by 0.1 for clarity.

Fig. 3,  $x = 0.019$  is the optimally doped composition, which has maximum  $T_c$  and largest shielding fraction. Both shielding fraction and  $T_c$  decrease with further Cu doping, and no diamagnetic signal above 2 K is detected in samples with the Cu doping level higher than 0.033.

Figure 4(a) presents the normal-state in-plane magnetic susceptibility for NaFe<sub>1-x</sub>Cu<sub>x</sub>As under a magnetic field of 5 T. The magnitude and behavior are similar to those in Co-doped NaFeAs.<sup>15</sup> Because the magnitude of  $\chi$  does not change much with the doping range up to 0.014 (about 15%), the normalized susceptibility is shown in Fig. 4(b) for clarity. All the magnetic susceptibilities are taken under zero-field-cooled (ZFC) mode, and a field-cooled (FC) susceptibility of NaFe<sub>0.70</sub>Cu<sub>0.30</sub>As is also presented. Rapid drops associated with superconducting transition can still be observed at low temperature for the superconducting samples. Kinks corresponding to the structural and SDW transitions are observed in the undoped and underdoped samples, which are suppressed with Cu doping and consistent with the observation of resistivity. It is worth noting that  $\chi$  shows an almost linear temperature dependence in high temperature for concentration up to 0.16. The slope of the linear dependence of high-temperature susceptibility slightly decreases with Cu doping, similar to that of Co doping.<sup>15</sup> The linear temperature dependence of high-temperature susceptibility is a common feature in iron-based superconductors, which has been observed in NaFe<sub>1-x</sub>Co<sub>x</sub>As,<sup>15</sup> Ba(Fe<sub>1-x</sub>Co<sub>x</sub>)<sub>2</sub>As<sub>2</sub>,<sup>26</sup> and LaFeAsO<sub>1-x</sub>F<sub>x</sub>.<sup>27</sup> An explanation based on the  $J_1$ - $J_2$  model of localized spins ascribes this behavior to the spin fluctuations arising from the local SDW correlation.<sup>28</sup> It is also argued that the behavior can be explained based on the spin susceptibility of a 2D Fermi liquid with nearly nested electron and hole pockets of the Fermi surface.<sup>29</sup> There is a Curie-Weiss-like upturn in the low-temperature magnetic susceptibility of

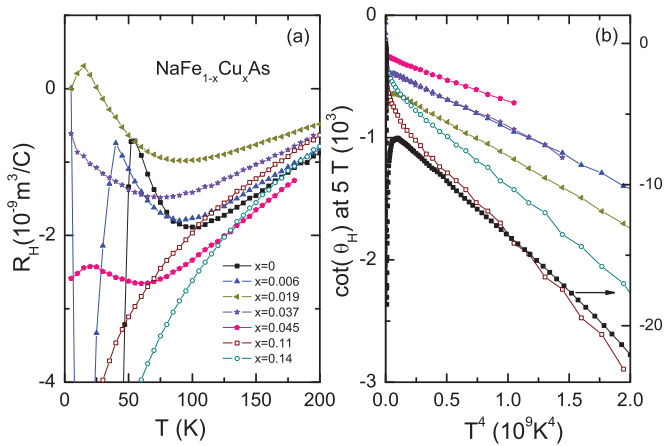


FIG. 5. (Color online) (a) Temperature dependence of the Hall coefficient  $R_H$  for selected  $\text{NaFe}_{1-x}\text{Cu}_x\text{As}$  single crystals. (b) The  $\cot\theta_H$  of  $\text{NaFe}_{1-x}\text{Cu}_x\text{As}$  single crystals plotted in power-law temperature scale. The legends in (b) are the same as in (a).

overdoped  $\text{NaFe}_{1-x}\text{Cu}_x\text{As}$ , which has been reported in many Fe-based superconductors.<sup>5,15,30,31</sup> The susceptibility upturn is usually attributed to extrinsic origin, such as defects or impurities. A small separation between the ZFC and FC occurs at  $\text{NaFe}_{0.70}\text{Cu}_{0.30}\text{As}$ , which can be ascribed to spin-glass transition.<sup>7</sup>

#### D. Hall effect

Figure 5(a) shows the temperature dependence of Hall coefficients for selected single crystals of  $\text{NaFe}_{1-x}\text{Cu}_x\text{As}$ . The drops in the  $x = 0$  and  $x = 0.006$  single crystals are due to structural transition. The negative Hall coefficients of all the single crystals indicate that the dominated carrier is electron. Taking contact sizes and geometric factor into account, the uncertain of the absolute value of Hall coefficient is about 15%. A nearly systematic evolution is observed on the absolute value of Hall coefficient at 200 K. The value decreases with Cu doping up to optimally doped crystal with  $x = 0.019$ , and then increases with further Cu doping. Due to the multiband effect and different mobility of electron and hole carriers, the Hall behavior is complex. If we simply take the single-band expression  $n_H = 1/(eR_H)$ ,<sup>32</sup> the behavior of Hall coefficient of  $\text{NaFe}_{1-x}\text{Cu}_x\text{As}$  indicates that the Cu doping is electron doping, similar to that of Co doping in  $\text{NaFe}_{1-x}\text{Co}_x\text{As}$ .<sup>15</sup> As the Cu doping, Hall coefficients of  $\text{Ba}_{0.6}\text{K}_{0.4}(\text{Fe}_{1-x}\text{Cu}_x)_2\text{As}_2$  gradually change from positive to negative values, clearly showing electron carriers are introduced. The results of Hall measurement on  $\text{NaFe}_{1-x}\text{Cu}_x\text{As}$  are similar to those of  $\text{Ba}_{0.6}\text{K}_{0.4}(\text{Fe}_{1-x}\text{Cu}_x)_2\text{As}_2$ .<sup>13</sup>

As shown in Fig. 5(b), the Hall angle is plotted as  $\cot\theta_H = \rho/\rho_{xy}$  vs  $T^4$ , where  $\rho$  is in-plane resistivity and  $\rho_{xy}$  is Hall resistivity. It has been reported that  $\cot\theta_H$  shows power-law temperature dependence for all the single crystals of  $\text{NaFe}_{1-x}\text{Co}_x\text{As}$ :  $T^4$  for the parent compound, approximately  $T^3$  for the superconducting crystals, and  $T^2$  for the heavily overdoped nonsuperconducting sample.<sup>19</sup> But  $T^\beta$ -dependent  $\cot\theta_H$  with  $\beta \approx 4$  is observed in all these  $\text{NaFe}_{1-x}\text{Cu}_x\text{As}$  single crystals. These  $\beta$ s are different from those in  $\text{NaFe}_{1-x}\text{Co}_x\text{As}$ ,  $\text{Ba}(\text{Fe}_{1-x}\text{Co}_x)_2\text{As}_2$ ,<sup>33</sup> and hole-doped cuprates,<sup>34</sup> but similar

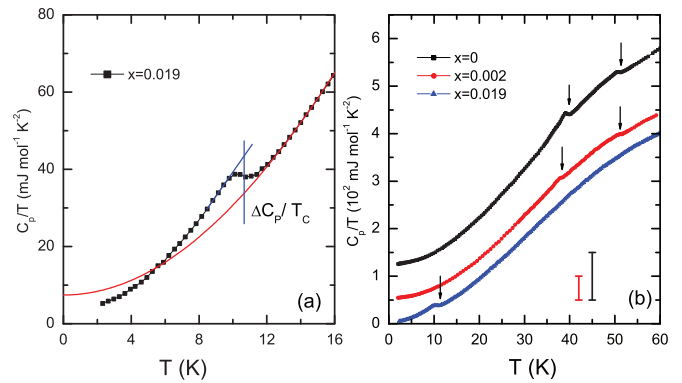


FIG. 6. (Color online) (a) Low-temperature part of specific heat for optimally doped  $\text{NaFe}_{0.981}\text{Cu}_{0.019}\text{As}$ . Blue lines show how the  $\Delta C_p/T_c$  is determined. The red line is the best fit of the specific heat between 13 and 30 K. (b) Temperature dependence of the specific heat  $C_p/T$  of  $\text{NaFe}_{1-x}\text{Cu}_x\text{As}$  with  $x = 0, 0.002$ , and  $0.019$  between 2 and 60 K. The data are shifted by a multiple of  $50 \text{ mJ mol}^{-1} \text{ K}^{-2}$  along the y axis for clarity (as shown in the panel). The arrows points to the anomalies in the specific heat.

to electron-doped cuprates.<sup>35</sup> Since the  $T^4$  dependence in cuprate is interpreted via the multiband effect with different contributions from various bands, the different power-law dependence between  $\text{NaFe}_{1-x}\text{Cu}_x\text{As}$  and  $\text{NaFe}_{1-x}\text{Co}_x\text{As}$  might indicate the different band evolution of  $\text{NaFeAs}$  by Cu/Co doping.

#### E. Specific heat

To verify the bulk thermodynamic nature of the superconducting transition, specific-heat measurement was performed on the optimally doped  $\text{NaFe}_{0.981}\text{Cu}_{0.019}\text{As}$ . As shown in Fig. 6(a), remarkable jump in specific heat corresponding to superconducting transition is observed, while no anomaly can be observed on the  $\text{NaFeAs}$  single crystal. The obvious jump in specific heat suggests that bulk superconductivity in  $\text{NaFeAs}$  is achieved by Cu doping.

The red line is the best fit of the normal-state specific heat between 13 and 30 K by  $C_p = \gamma_n T + \beta T^3 + \eta T^5$ , where  $\gamma_n T$  and  $\beta T^3 + \eta T^5$  are electron and phonon contributions, respectively. The  $T^3$  term is the phonon specific heat produced by the Debye model, and the  $T^5$  term is the second term of the harmonic-lattice approximation, which is added to improve the fit of phonon specific heat as often reported in other iron-based superconductors.<sup>36–39</sup> It is found that  $\gamma_n = 7.44 \text{ mJ mol}^{-1} \text{ K}^{-2}$ ,  $\beta = 0.238 \text{ mJ mol}^{-1} \text{ K}^{-4}$ , and  $\eta = -5.00 \times 10^{-5} \text{ mJ mol}^{-1} \text{ K}^{-6}$ . From the obtained  $\beta$  and by using the formula  $\Theta_D = [12\pi^4 k_B N_A Z / (5\beta)]^{1/3}$ , where  $N_A$  is the Avogadro constant,  $k_B$  is the Boltzmann constant, and  $Z$  is the total number of atoms in one unit cell, the Debye temperature ( $\Theta_D$ ) is estimated to be 290 K, resembling to that of  $\text{NaFe}_{0.972}\text{Co}_{0.028}\text{As}$ .<sup>15</sup>  $\Delta C_p/T_c$  at  $T_c = 10.65 \text{ K}$  is estimated to be  $9.85 \text{ mJ mol}^{-1} \text{ K}^{-2}$  by the isentropic construction sketched in Fig. 6(a). The obtained  $\Delta C_p/T_c$  agrees with the value predicted by the expanded BNC scaling, which is proposed by Bud'ko, Ni, and Canfield (BNC) and expanded by J. S. Kim *et al.*<sup>40,41</sup> It is regarded that the BNC scaling represents a general property of a large class

of iron-based superconductors, and serves as a simple test of whether a superconductor has the same superconducting pairing mechanism as the typical iron-based superconductors.<sup>42,43</sup> Thus, the agreement with BNC trend suggests that NaFe<sub>0.981</sub>Cu<sub>0.019</sub>As has a typical pairing mechanism of iron-based superconductors, just as Ba(Fe<sub>0.925</sub>Co<sub>0.075</sub>)<sub>2</sub>As<sub>2</sub> and NaFe<sub>0.972</sub>Co<sub>0.028</sub>As.<sup>15,44</sup> It has been reported that  $\Delta C_p/\gamma_n T_c = 2.11$  in NaFe<sub>0.972</sub>Co<sub>0.028</sub>As.<sup>15</sup> Based on the data obtained above,  $\Delta C_p/\gamma_n T_c$  in NaFe<sub>0.981</sub>Cu<sub>0.019</sub>As is estimated to be 1.32, a little smaller than 1.43 expected for weak-coupling BCS superconductor. The different values of  $\Delta C_p/\gamma_n T_c$  between optimally Cu- and Co-doped NaFeAs suggest that the coupling strength in Cu-doped NaFeAs is weaker than that of the Co-doped sample. As a result, NaFe<sub>0.981</sub>Cu<sub>0.019</sub>As should be a two-band *s*-wave superconductor with a weak coupling strength.

The temperature dependence of specific heats taken from 2 to 60 K is presented in Fig. 6(b) for NaFe<sub>1-x</sub>Cu<sub>x</sub>As with  $x = 0, 0.002, 0.019$ . Two anomalies corresponding to structural and SDW transitions can be clearly observed in the underdoped samples,<sup>45</sup> but no kink is observed around  $T_c$ , which is consistent with the tiny shielding fraction from the susceptibility measurements shown in Fig. 3. With Cu doping, these two anomalies are suppressed to lower temperature, and become obscure, eventually indiscernible with  $x > 0.002$ . In the optimally doped NaFe<sub>0.981</sub>Cu<sub>0.019</sub>As, only a kink associated with superconducting transition is observed. The evolution of specific heat clearly shows that the structural and SDW transitions are suppressed and superconductivity is enhanced by Cu doping.

### F. Phase diagram

The resistivity, specific-heat, Hall, and magnetic-susceptibility measurements all show the suppression of the structural and SDW transitions. In order to quantify the transitions and compare the transitions inferred from various measurements, the resistivity, specific-heat, Hall, and magnetic-susceptibility data of NaFeAs are plotted in Fig. 7 with the same temperature scale. The criteria used to define the  $T_s^\rho$  and  $T_{SDW}^\rho$  from resistivity are shown in Fig. 7(a). The onsets of specific-heat jumps are used to define  $T_s^{C_p}$  and  $T_{SDW}^{C_p}$ .  $R_H$  starts to drop at  $T_s^{R_H}$  and drops quickly at  $T_{SDW}^{R_H}$ . Similarly to  $R_H$ ,  $\chi$  starts to drop at  $T_s^\chi$  and forms a small peak at  $T_{SDW}^\chi$ . As shown in Figs. 7 and 8,  $T_s$ s and  $T_{SDW}$ s inferred from various measurements are in excellent agreement with each other. It is noteworthy that neither specific heat nor magnetic susceptibility shows a kink corresponding to the superconducting transition, which is consistent with the filamentary superconductivity proposed before.<sup>22</sup>

Based on the data of resistivity, magnetic-susceptibility, Hall, and specific-heat measurements obtained so far, the  $T$ - $x$  phase diagram of NaFe<sub>1-x</sub>Cu<sub>x</sub>As is plotted in Fig. 8. As the Cu doping, both structural and SDW transitions are progressively suppressed to low temperature, and  $T_c$  is enhanced slightly from 9.6 K in NaFeAs to 11.5 K in optimally Cu-doped NaFeAs.  $T_c$  decreases with further Cu doping, and the metal-insulator transition is observed in the normal-state resistivity of overdoped superconducting samples. Extremely overdoped samples exhibit semiconducting behavior, which is different

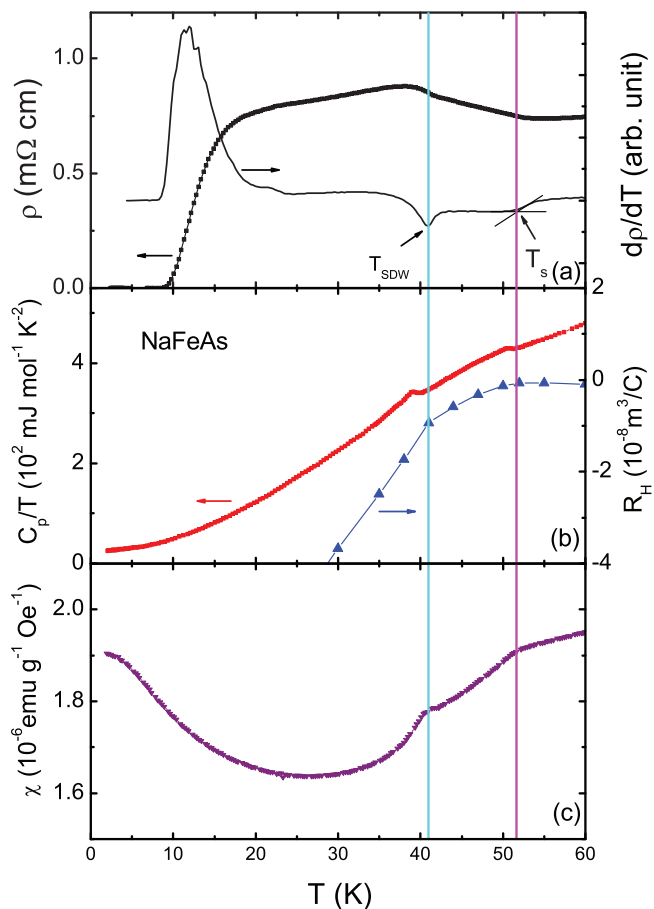


FIG. 7. (Color online) Criteria used to determine the structural transition  $T_s$  and SDW transition  $T_{SDW}$  of NaFeAs. (a) Resistivity and its derivative. (b) Specific heat and Hall coefficient. (c) Magnetic susceptibility. Vertical lines are inferred from the  $d\rho/dT$ .

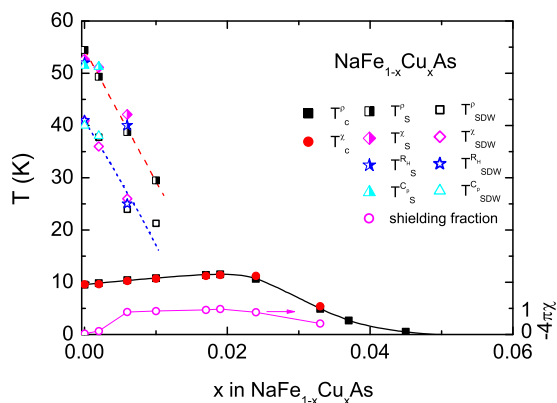


FIG. 8. (Color online)  $T$ - $x$  phase diagram of NaFe<sub>1-x</sub>Cu<sub>x</sub>As. Filled, half-filled, and open symbols represent superconducting transition ( $T_c$ ), structural transition ( $T_s$ ), and SDW transition ( $T_{SDW}$ ), respectively. Squares, stars, and triangles are data inferred from resistivity, Hall, and specific-heat measurements, respectively. The filled red circles and diamonds are the data inferred from the magnetic susceptibility taken with magnetic field 10 Oe and 5 T, respectively. Magenta open circles represent the shielding fraction inferred from Fig. 3. Lines are guides to the eye.

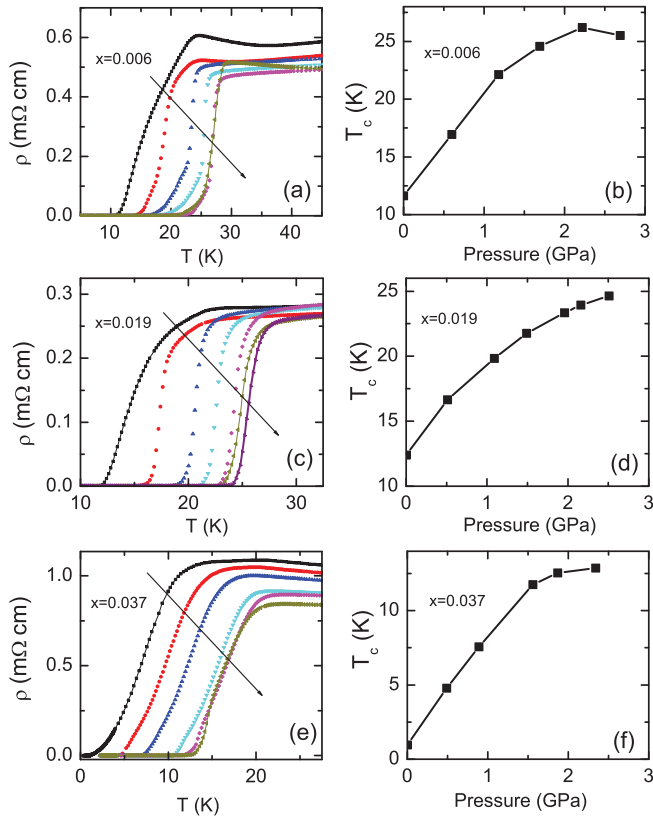


FIG. 9. (Color online) Left panels: In-plane resistivity of  $\text{NaFe}_{1-x}\text{Cu}_x\text{As}$  [ $x = 0.006$  (a),  $0.019$  (c), and  $0.037$  (e)] under various pressures; arrows indicate the direction of the increasing pressure. Right panels: The  $T(p)$  phase diagrams of the samples corresponding to the left panels.

from the overdoped nonsuperconducting  $\text{NaFe}_{1-x}\text{Co}_x\text{As}$ , where metallic behavior is observed. A weak semiconducting behavior is also observed in overdoped  $\text{Ba}(\text{Fe}_{1-x}\text{Cu}_x)_2\text{As}_2$  and  $\text{Sr}(\text{Fe}_{1-x}\text{Cu}_x)_2\text{As}_2$ .<sup>5,7</sup> Although the magnitude of  $T_c$  enhancement of  $\text{NaFeAs}$  is only 1.9 K by Cu doping, as shown in Fig. 8, the negligible small shielding fraction is enhanced to nearly 100% at optimally doped  $x = 0.019$ . The shielding fraction decreases with further Cu doping, and a dome-like temperature dependence of shielding fraction is observed, which is similar to the doping dependence of  $T_c$  in  $\text{Ba}(\text{Fe}_{1-x}\text{Co}_x)_2\text{As}_2$ . The full shielding fraction around optimally doped  $\text{NaFe}_{1-x}\text{Cu}_x\text{As}$  indicates that Cu doping is beneficial for the superconductivity of  $\text{NaFeAs}$ , in contrast to the case of  $\text{LiFe}_{1-x}\text{Co}_x\text{As}$ .<sup>16</sup> But the maximum  $T_c$  is obviously lower than 20 K in  $\text{NaFe}_{1-x}\text{Co}_x\text{As}$  under ambient pressure; the maximum  $T_c$  may be suppressed by the stronger impurity potential of Cu. Microscopic coexistence of SDW and superconductivity has been proved by scanning tunneling microscopy (STM) and ARPES measurements on underdoped  $\text{NaFe}_{1-x}\text{Co}_x\text{As}$ .<sup>46,47</sup> Considering the similarity between Cu and Co doping effects, it is likely that superconductivity also coexists with SDW in the underdoped  $\text{NaFe}_{1-x}\text{Cu}_x\text{As}$ .

### G. Pressure effects

Resistivity measurements under pressure were performed on the underdoped sample with  $x = 0.006$ , optimally doped

$x = 0.019$ , and overdoped  $x = 0.037$  samples. As shown in Fig. 9(a), for the underdoped single crystal with  $x = 0.006$ , the resistivity upturn associated with the structural or SDW transition is suppressed to lower temperature by pressure and eventually becomes indistinguishable.  $T_c$  initially increases as the pressure, and maximum transition temperature  $T_c^{\text{max}} = 26.2$  K is observed at 2.2 GPa,<sup>48</sup>  $T_c$  decreases with further increasing pressure, and the data are summarized in Fig. 9(b). For optimally doped and overdoped samples, where structural and SDW transitions have been suppressed by Cu doping,  $T_c$ s are monotonically enhanced up to the maximum pressure in our measurements.

As shown in Figs. 9(d) and 9(f),  $T_c^{\text{max}} = 24.6$  and 12.9 K are obtained for  $x = 0.019$  and  $x = 0.037$ , respectively. The magnitudes of  $\Delta T_c$  enhanced by  $\sim 2.2$  GPa are about 13.9, 12.2, and 11.9 K for  $x = 0.006$ , 0.019, and 0.037, respectively, which are comparable to that of  $\text{NaFe}_{1-x}\text{Co}_x\text{As}$ .<sup>49</sup> It is reported that the pressure medium (Daphne 7373) solidifies at 2.2 GPa,<sup>48</sup> which is considered as the hydrostatic limit.<sup>50</sup> As shown in Fig. 9, the superconducting transition width is relatively narrow under maximum pressure ( $\sim 2.2$  GPa), so the pressure in our measurements is homogeneous, and the nonhydrostatic pressure effect, if any, is small.

The  $T_c^{\text{max}}$ s of  $\text{NaFe}_{1-x}\text{Co}_x\text{As}$  and  $\text{NaFe}_{1-x}\text{Cu}_x\text{As}$  obtained under pressure are plotted in Fig. 10. As shown in Fig. 10, the maximum  $T_c$  obtained by combining the effect of doping and pressure in  $\text{NaFe}_{1-x}\text{Cu}_x\text{As}$  decreases with Cu concentration, in contrast to the pressure effect on  $\text{NaFe}_{1-x}\text{Co}_x\text{As}$ , where maximum  $T_c$ s of about 31 K are observed from undoped to optimally doped samples.<sup>49</sup> Substitution of Fe by other transition metals can induce carriers as well as impurities. Considering the similarity of the carrier doping effect between Cu and Co, it is mainly the impurity effect that is responsible for the different doping dependence of  $T_c^{\text{max}}$ . If we only consider the impurity effect on the maximum transition temperature of  $\text{NaFeAs}$ , the magnitude of  $\Delta T_c^{\text{max}}$  suppressed by  $\sim 4\%$  Cu doping in  $\text{NaFe}_{1-x}\text{Cu}_x\text{As}$  is about 18 K, slightly larger than  $\sim 14$  K in  $\text{Ba}_{0.6}\text{K}_{0.4}(\text{Fe}_{1-x}\text{Cu}_x)_2\text{As}_2$ ,<sup>13</sup> but much larger than  $\sim 2$  K in  $\text{NaFe}_{1-x}\text{Co}_x\text{As}$ . The larger superconducting suppression effect of Cu suggests that the impurity potential of Cu is stronger than that of Co in  $\text{NaFeAs}$ .

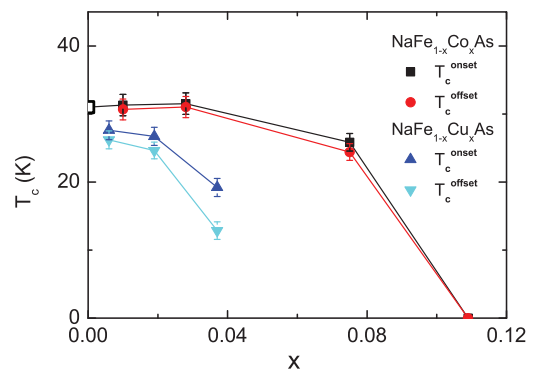


FIG. 10. (Color online)  $T_c^{\text{max}}$  of  $\text{NaFe}_{1-x}\text{Co}_x\text{As}$  and  $\text{NaFe}_{1-x}\text{Cu}_x\text{As}$  plotted as functions of the Co/Cu substitution,  $x$ . The open black symbol represents the  $T_c^{\text{max}}$  of  $\text{NaFeAs}$  reported by Zhang *et al.* (Ref. 55). The data of  $\text{NaFe}_{1-x}\text{Co}_x\text{As}$  are taken from Ref. 49.

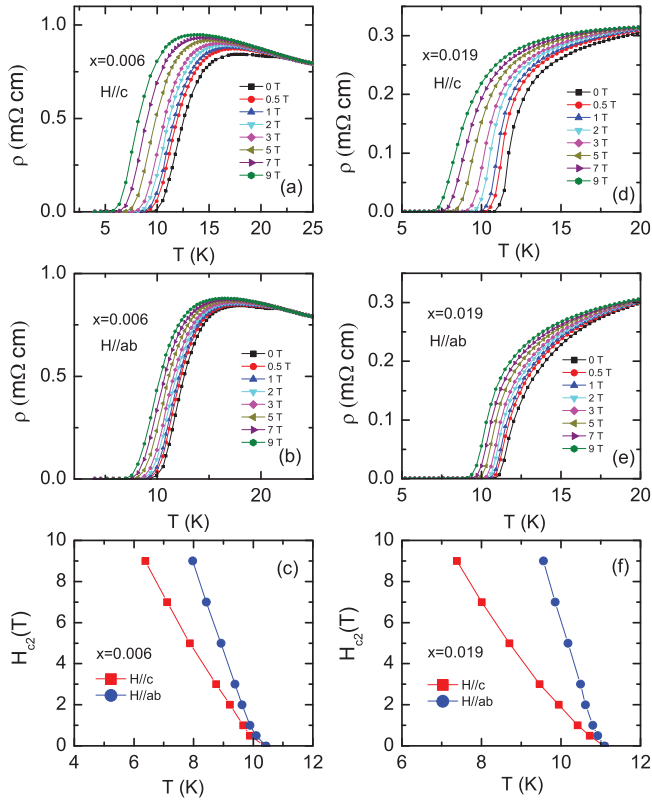


FIG. 11. (Color online) The temperature dependence of resistivity for underdoped NaFe<sub>0.994</sub>Cu<sub>0.006</sub>As [(a) and (b)] and optimally doped NaFe<sub>0.981</sub>Cu<sub>0.019</sub>As [(d) and (e)] crystals with the magnetic field parallel and perpendicular to the *c* axis, respectively. (c) and (f) The temperature dependence of  $H_{c2}$  for NaFe<sub>0.994</sub>Cu<sub>0.006</sub>As and NaFe<sub>0.981</sub>Cu<sub>0.019</sub>As, respectively.

### H. Anisotropy of the upper critical field

In Fig. 11, we present the temperature dependence of resistivity for NaFe<sub>1-x</sub>Cu<sub>x</sub>As ( $x = 0.006, 0.019$ ) under various magnetic fields. The transition temperature of superconductivity [the criterion is shown in Fig. 2(d)] is suppressed gradually and the transition is broadened with increasing magnetic field. The effect of magnetic field is much larger when the field is applied along the *c* axis of the single crystals than that of within the *ab* plane. For underdoped NaFe<sub>0.994</sub>Cu<sub>0.006</sub>As, the positive magnetoresistance appears well below the temperature which is defined as the SDW transition. A similar phenomenon was also observed in NaFeAs single crystals.<sup>45</sup> Temperature-dependent  $H_{c2}$  curves for NaFe<sub>0.994</sub>Cu<sub>0.006</sub>As and NaFe<sub>0.981</sub>Cu<sub>0.019</sub>As are shown in Figs. 11(c) and 11(f), respectively. In order to determine the upper critical field in the low-temperature region, we adopt the Werthamer-Helfand-Hohenberg (WHH) formula  $H_{c2}(0) = 0.693[-(dH_{c2}/dT)]_{T_c}T_c$  for single-band BCS superconductors. We obtain  $[-(dH_{c2}^{ab}/dT)]_{T_c} = 4.23$  T/K and  $[-(dH_{c2}^c/dT)]_{T_c} = 2.24$  T/K at  $T_c = 10.40$  K from Fig. 11(c) for NaFe<sub>0.994</sub>Cu<sub>0.006</sub>As, so  $H_{c2}(0)$  can be estimated to be 30 and 16 T with the field parallel and perpendicular to the *ab* plane, respectively. In the same way,  $H_{c2}^{ab}(0) = 49$  T and  $H_{c2}^c(0) = 22$  T are obtained for the NaFe<sub>0.981</sub>Cu<sub>0.019</sub>As single crystal. As a result, the anisotropy parameter  $\gamma_H = H_{c2}^{ab}(0)/H_{c2}^c(0)$  can

be estimated to be 1.88 and 2.22 for NaFe<sub>0.994</sub>Cu<sub>0.006</sub>As and NaFe<sub>0.981</sub>Cu<sub>0.019</sub>As, respectively. The smaller anisotropy  $\gamma_H$  in underdoped samples than those in the overdoped samples has also been observed in Ba(Fe<sub>1-x</sub>Co<sub>x</sub>)<sub>2</sub>As<sub>2</sub>, where  $\sim 50\%$  smaller anisotropy was found in underdoped region.<sup>51</sup> These anisotropy values are close to those in NaFe<sub>1-x</sub>Co<sub>x</sub>As (2.25–2.35),<sup>21</sup> and a little larger than those in Ba<sub>0.60</sub>K<sub>0.40</sub>Fe<sub>2</sub>As<sub>2</sub> and the Fe(Se, Te) system (1.7–1.86),<sup>52,53</sup> but smaller than those in NdFeAsO<sub>1-x</sub>F<sub>x</sub> (5–9).<sup>54</sup>

## IV. DISCUSSION

The overall phase diagram of NaFe<sub>1-x</sub>Cu<sub>x</sub>As is similar to those of NaFe<sub>1-x</sub>Co<sub>x</sub>As and Ba(Fe<sub>1-x-y</sub>Co<sub>x</sub>Cu<sub>y</sub>)<sub>2</sub>As<sub>2</sub> ( $x \sim 0.022$  and  $0.047$ ),<sup>5,15</sup> which indicates that the carrier doping effect between Cu and Co is similar. As a result, the Cu doping definitely introduces electron carriers into NaFe<sub>1-x</sub>Cu<sub>x</sub>As as in the case of Co doping. The main difference between Cu- and Co-doped NaFeAs lies in that the semiconducting instead of the metallic phase is observed in the extremely overdoped samples, indicating that the impurity effect of Cu is different from that of Co in NaFeAs.

According to the comparison of the phase diagrams for Ba(Fe<sub>1-x</sub>TM<sub>x</sub>)<sub>2</sub>As<sub>2</sub> ( $TM = \text{Co, Ni, Cu, and Co/Cu}$ ), the narrow superconducting dome of Ba(Fe<sub>1-x</sub>Cu<sub>x</sub>)<sub>2</sub>As<sub>2</sub> has been interpreted that too many electrons have been added when the structural/antiferromagnetic phase transitions are suppressed low enough.<sup>5</sup> But recent ARPES results on Ba(Fe<sub>1-x</sub>TM<sub>x</sub>)<sub>2</sub>As<sub>2</sub> ( $TM = \text{Co, Ni, and Cu}$ ) suggest that although electrons are indeed doped, part of them may be localized and do not fill the energy bands as predicted by the rigid-band model.<sup>6</sup> Theory calculation found that the substitution with strong impurity potential induces an impurity band split-off below the original host band, which reduces the electron occupation from the host band and results in a decrease of the electron occupation.<sup>56–58</sup> As a result, both theory and experiment show that the number of electrons doped by Cu is less than the value expected from the simple rigid-band model.

ARPES and density functional theory (DFT) studies found that the impurity potential of the substituted atoms enhances from Co, Ni, to Cu.<sup>6,56,59</sup> As also suggested by high-pressure measurement, the impurity effect of Cu is stronger than that of Co. The width of the superconducting dome is mainly controlled by the balance of carrier concentration and impurity scattering induced by the dopants. So the narrow or even absence of the superconducting dome in the phase diagram of Cu-doped BaFe<sub>2</sub>As<sub>2</sub> arises from that too many impurities are induced when enough carriers are doped. Therefore, the wider superconducting dome of Ba(Fe<sub>1-x-y</sub>Co<sub>x</sub>Cu<sub>y</sub>)<sub>2</sub>As<sub>2</sub> ( $x \sim 0.022$  and  $0.047$ ) than that of Ba(Fe<sub>1-x</sub>Cu<sub>x</sub>)<sub>2</sub>As<sub>2</sub> can be understood that fewer carriers are needed when BaFe<sub>2</sub>As<sub>2</sub> has already been electron doped by Co, while in NaFeAs, whose structural/SDW transition temperature is much lower than that of BaFe<sub>2</sub>As<sub>2</sub>, fewer electrons are required to suppress SDW and induce superconductivity. Therefore, Cu doping can provide enough carriers to map out a phase diagram similar to NaFe<sub>1-x</sub>Co<sub>x</sub>As and Ba(Fe<sub>1-x</sub>Co<sub>x</sub>)<sub>2</sub>As<sub>2</sub>. Meanwhile, as the Cu concentration further increases, density of states (DOS) at  $E_F$  is gradually removed by the impurity band induced by Cu

doping. As a result, semiconductor-like behavior finally shows up in  $\text{NaFe}_{1-x}\text{Cu}_x\text{As}$ .

This scenario can also explain the contradiction between the results of XPS/XAS and ARPES. Since Cu  $3d$  states are located deeper below the  $E_F$  than Co,<sup>6,9,56</sup> the extra  $d$  electrons for Cu almost totally locate around the substituted site. Hence, a closed  $3d$  shell is observed with XPS and XAS, though there are a few delocalized electrons introduced by the Cu dopant. It is found that substitutions of Cu for Fe in  $(\text{Ba}, \text{Sr})\text{Fe}_2\text{As}_2$  at low level results in electron doping, while  $\text{SrCu}_2\text{As}_2$ , the end member of  $\text{Sr}(\text{Fe}_{1-x}\text{Cu}_x)_2\text{As}_2$ , is an  $sp$ -band metal with hole-type carriers dominant.<sup>6,7,11</sup> The contradictory result has been interpreted that there is a crossover between electron and hole doping with increasing  $x$ , which is induced by tetragonal (T) to collapsed tetragonal (cT) phase transition as a function of doping.<sup>11</sup> Thus, in the case of  $\text{NaFe}_{1-x}\text{Cu}_x\text{As}$ , where no cT phase has been observed, it is natural to observe electron doping at low-level substitution of Cu for Fe.

## V. SUMMARY AND CONCLUSIONS

In conclusion, we have performed structural, transport, thermodynamic, and high-pressure measurements on  $\text{NaFe}_{1-x}\text{Cu}_x\text{As}$  single crystals. Enough carriers can be provided by Cu doping to map out a phase diagram similar to  $\text{NaFe}_{1-x}\text{Co}_x\text{As}$ . In the underdoped region, both the structural

and SDW transition are monotonically suppressed by Cu doping.  $T_c$  and the superconducting shielding fraction are enhanced with the doping. Bulk superconductivity with  $T_c = 11.5$  K is observed at the optimally doped sample, and  $T_c$  decreases with further doping. Finally, semiconducting instead of metallic behavior in  $\text{NaFe}_{1-x}\text{Co}_x\text{As}$  is observed in extremely overdoped nonsuperconducting samples.  $T_c$  is obviously enhanced by pressure, but  $T_c^{\text{max}}$  decreases faster by Cu doping case than that of Co doping, indicating that Cu doping would induce stronger impurity scattering than that of Co doping in  $\text{NaFeAs}$ . The Hall measurements and comparison between Cu- and Co-doped  $\text{NaFeAs}$  phase diagrams indicate that Cu doping introduces electrons into system, but the number of electrons is far from  $3x$  as predicted by the rigid-band model.

## ACKNOWLEDGMENTS

This work is supported by the National Natural Science Foundation of China (Grants No. 11190021, No. 11174266, No. 51021091), the ‘‘Strategic Priority Research Program (B)’’ of the Chinese Academy of Sciences (Grant No. XDB04040100), the National Basic Research Program of China (973 Program, Grants No. 2012CB922002 and No. 2011CBA00101), and the Chinese Academy of Sciences.

\*Corresponding author: chenxh@ustc.edu.cn

- <sup>1</sup>Y. Kamihara, T. Watanabe, M. Hirano, and H. Hosono, *J. Am. Chem. Soc.* **130**, 3296 (2008).  
<sup>2</sup>X. H. Chen, T. Wu, G. Wu, R. H. Liu, H. Chen, and D. F. Fang, *Nature (London)* **453**, 761 (2008).  
<sup>3</sup>M. Rotter, M. Tegel, and D. Johrendt, *Phys. Rev. Lett.* **101**, 107006 (2008).  
<sup>4</sup>A. S. Sefat, R. Jin, M. A. McGuire, B. C. Sales, D. J. Singh, and D. Mandrus, *Phys. Rev. Lett.* **101**, 117004 (2008).  
<sup>5</sup>N. Ni, A. Thaler, J. Q. Yan, A. Kracher, E. Colombier, S. L. Bud’ko, P. C. Canfield, and S. T. Hannahs, *Phys. Rev. B* **82**, 024519 (2010).  
<sup>6</sup>S. Ideta, T. Yoshida, I. Nishi, A. Fujimori, Y. Kotani, K. Ono, Y. Nakashima, S. Yamaichi, T. Sasagawa, M. Nakajima, K. Kihou, Y. Tomioka, C. H. Lee, A. Iyo, H. Eisaki, T. Ito, S. Uchida, and R. Arita, *Phys. Rev. Lett.* **110**, 107007 (2013).  
<sup>7</sup>Y. J. Yan, P. Cheng, J. J. Ying, X. G. Luo, F. Chen, H. Y. Zou, A. F. Wang, G. J. Ye, Z. J. Xiang, J. Q. Ma, and X. H. Chen, *Phys. Rev. B* **87**, 075105 (2013).  
<sup>8</sup>M. Merz, P. Schweiss, P. Nagel, Th. Wolf, H. v. Löhneysen, and S. Schuppler, arXiv:1306.4222.  
<sup>9</sup>J. A. McLeod, A. Buling, R. J. Green, T. D. Boyko, N. A. Skorikov, E. Z. Kurmaev, M. Neumann, L. D. Finkelstein, N. Ni, A. Thaler, S. L. Bud’ko, P. C. Canfield, and A. Moewes, *J. Phys.: Condens. Matter* **24**, 215501 (2012).  
<sup>10</sup>D. J. Singh, *Phys. Rev. B* **79**, 153102 (2009).  
<sup>11</sup>V. K. Anand, P. K. Perera, A. Pandey, R. J. Goetsch, A. Kreyssig, and D. C. Johnston, *Phys. Rev. B* **85**, 214523 (2012).  
<sup>12</sup>A. Thaler, H. Hodovanets, M. S. Torikachvili, S. Ran, A. Kracher, W. Straszheim, J. Q. Yan, E. Mun, and P. C. Canfield, *Phys. Rev. B* **84**, 144528 (2011).

- <sup>13</sup>P. Cheng, B. Shen, F. Han, and H. H. Wen, arXiv:1304.4568.  
<sup>14</sup>D. R. Parker, M. J. P. Smith, T. Lancaster, A. J. Steele, I. Franke, P. J. Baker, F. L. Pratt, M. J. Pitcher, S. J. Blundell, and S. J. Clarke, *Phys. Rev. Lett.* **104**, 057007 (2010).  
<sup>15</sup>A. F. Wang, X. G. Luo, Y. J. Yan, J. J. Ying, Z. J. Xiang, G. J. Ye, P. Cheng, Z. Y. Li, W. J. Hu, and X. H. Chen, *Phys. Rev. B* **85**, 224521 (2012).  
<sup>16</sup>L. Y. Xing, X. C. Wang, Z. Deng, Q. Q. Liu, and C. Q. Jin, *Physica C* **493**, 141 (2013).  
<sup>17</sup>M. A. Tanatar, N. Spyrison, Kyuil Cho, E. C. Blomberg, Guotai Tan, Pengcheng Dai, Chenglin Zhang, and R. Prozorov, *Phys. Rev. B* **85**, 014510 (2012).  
<sup>18</sup>S. Y. Zhou, X. C. Hong, X. Qiu, B. Y. Pan, Z. Zhang, X. L. Li, W. N. Dong, A. F. Wang, X. G. Luo, X. H. Chen, and S. Y. Li, *Europhys. Lett.* **101**, 17007 (2013).  
<sup>19</sup>A. F. Wang, J. J. Ying, X. G. Luo, Y. J. Yan, D. Y. Liu, Z. J. Xiang, P. Cheng, G. J. Ye, L. J. Zou, Z. Sun, and X. H. Chen, *New J. Phys.* **15**, 043048 (2013).  
<sup>20</sup>A. Eiling and J. S. Schilling, *J. Phys. F: Met. Phys.* **11**, 623 (1981).  
<sup>21</sup>N. Spyrison, M. A. Tanatar, K. Cho, Y. Song, P. C. Dai, C. L. Zhang, and R. Prozorov, *Phys. Rev. B* **86**, 144528 (2012).  
<sup>22</sup>S. L. Li, C. de la Cruz, Q. Huang, G. F. Chen, T.-L. Xia, J. L. Luo, N. L. Wang, and P. C. Dai, *Phys. Rev. B* **80**, 020504(R) (2009).  
<sup>23</sup>A. J. Williams, T. M. McQueen, V. Ksenofontov, C. Felser, and R. J. Cava, *J. Phys.: Condens. Matter* **21**, 305701 (2009).  
<sup>24</sup>Tzu-Wen Huang, Ta-Kun Chen, Kuo-Wei Yeh, Chung-Ting Ke, Chi Liang Chen, Yi-Lin Huang, Fong-Chi Hsu, Maw-Kuen Wu, Phillip M. Wu, Maxim Avdeev, and Andrew J. Studer, *Phys. Rev. B* **82**, 104502 (2010).

- <sup>25</sup>Stanislav Chadov, Daniel Schärff, Gerhard H. Fecher, Claudia Felser, L. J. Zhang, and D. J. Singh, *Phys. Rev. B* **81**, 104523 (2010).
- <sup>26</sup>X. F. Wang, T. Wu, G. Wu, R. H. Liu, H. Chen, Y. L. Xie, and X. H. Chen, *New J. Phys.* **11**, 045003 (2009).
- <sup>27</sup>R. Klingeler, N. Leps, I. Hellmann, A. Popa, U. Stockert, C. Hess, V. Kataev, H.-J. Grafe, F. Hammerath, G. Lang, S. Wurmehl, G. Behr, L. Harnagea, S. Singh, and B. Büchner, *Phys. Rev. B* **81**, 024506 (2010).
- <sup>28</sup>G. M. Zhang, Y. H. Su, Z. Y. Lu, Z. Y. Weng, D. H. Lee, and T. Xiang, *Europhys. Lett.* **86**, 37006 (2009).
- <sup>29</sup>M. M. Korshunov, I. Eremin, D. V. Efremov, D. L. Maslov, and A. V. Chubukov, *Phys. Rev. Lett.* **102**, 236403 (2009).
- <sup>30</sup>Z. J. Xiang, X. G. Luo, J. J. Ying, X. F. Wang, Y. J. Yan, A. F. Wang, P. Cheng, G. J. Ye, and X. H. Chen, *Phys. Rev. B* **85**, 224527 (2012).
- <sup>31</sup>G. H. Cao, S. Jiang, X. Lin, C. Wang, Y. K. Li, Z. Ren, Q. Tao, C. M. Feng, J. H. Dai, Z. A. Xu, and F. C. Zhang, *Phys. Rev. B* **79**, 174505 (2009).
- <sup>32</sup>F. Rullier-Albenque, D. Colson, A. Forget, and H. Alloul, *Phys. Rev. Lett.* **103**, 057001 (2009).
- <sup>33</sup>E. Arushanov, S. Levchenko, G. Fuchs, B. Holzapfel, S. L. Drechsler, and L. Schultz, *J. Supercond. Nov. Magn.* **24**, 2285 (2011).
- <sup>34</sup>T. R. Chien, Z. Z. Wang, and N. P. Ong, *Phys. Rev. Lett.* **67**, 2088 (1991).
- <sup>35</sup>C. H. Wang, G. Y. Wang, T. Wu, Z. Feng, X. G. Luo, and X. H. Chen, *Phys. Rev. B* **72**, 132506 (2005).
- <sup>36</sup>T. H. K. Barron and J. A. Morrison, *Can. J. Phys.* **35**, 799-810 (1957).
- <sup>37</sup>S. B. Lang, W. M. Zhu, and Z.-G. Ye, *J. Appl. Phys.* **111**, 094102 (2012).
- <sup>38</sup>Ch. Wälti, E. Felder, C. Degen, G. Wigger, R. Monnier, B. Delley, and H. R. Ott, *Phys. Rev. B* **64**, 172515 (2001).
- <sup>39</sup>Dong-Jin Jang, J. B. Hong, Y. S. Kwon, T. Park, K. Gofryk, F. Ronning, J. D. Thompson, and Yunkyu Bang, *Phys. Rev. B* **85**, 180505(R) (2012).
- <sup>40</sup>S. L. Bud'ko, N. Ni, and P. C. Canfield, *Phys. Rev. B* **79**, 220516 (2009).
- <sup>41</sup>J. S. Kim, G. R. Stewart, S. Kasahara, T. Shibauchi, T. Terashima, and Y. Matsuda, *J. Phys.: Condens. Matter* **23**, 222201 (2011).
- <sup>42</sup>G. R. Stewart, *Rev. Mod. Phys.* **83**, 1589 (2011).
- <sup>43</sup>J. S. Kim, L. Y. Xing, X. C. Wang, C. Q. Jin, and G. R. Stewart, *Phys. Rev. B* **87**, 054504 (2013).
- <sup>44</sup>F. Hardy, T. Wolf, R. A. Fisher, R. Eder, P. Schweiss, P. Adelman, H. v. Löhneysen, and C. Meingast, *Phys. Rev. B* **81**, 060501(R) (2010).
- <sup>45</sup>G. F. Chen, W. Z. Hu, J. L. Luo, and N. L. Wang, *Phys. Rev. Lett.* **102**, 227004 (2009).
- <sup>46</sup>P. Cai, X. D. Zhou, W. Ruan, A. F. Wang, X. H. Chen, D. H. Lee, and Y. Y. Wang, *Nat. Commun.* **4**, 1596 (2013).
- <sup>47</sup>Q. Q. Ge, Z. R. Ye, M. Xu, Y. Zhang, J. Jiang, B. P. Xie, Y. Song, C. L. Zhang, Pengcheng Dai, and D. L. Feng, *Phys. Rev. X* **3**, 011020 (2013).
- <sup>48</sup>K. Yokogawa, K. Murata, H. Yoshino, and S. Aoyama, *Jpn. J. Appl. Phys.* **46**, 3636 (2007).
- <sup>49</sup>A. F. Wang, Z. J. Xiang, J. J. Ying, Y. J. Yan, P. Cheng, G. J. Ye, X. G. Luo, and X. H. Chen, *New J. Phys.* **14**, 113043 (2012).
- <sup>50</sup>S. K. Kim, M. S. Torikachvili, E. Colombier, A. Thaler, S. L. Bud'ko, and P. C. Canfield, *Phys. Rev. B* **84**, 134525 (2011).
- <sup>51</sup>N. Ni, M. E. Tillman, J.-Q. Yan, A. Kracher, S. T. Hannahs, S. L. Bud'ko, and P. C. Canfield, *Phys. Rev. B* **78**, 214515 (2008).
- <sup>52</sup>H. Q. Yuan, J. Singleton, F. F. Balakirev, S. A. Baily, G. F. Chen, J. L. Luo, and N. L. Wang, *Nature (London)* **457**, 565 (2009).
- <sup>53</sup>M. H. Fang, J. H. Yang, F. F. Balakirev, Y. Kohama, J. Singleton, B. Qian, Z. Q. Mao, H. D. Wang, and H. Q. Yuan, *Phys. Rev. B* **81**, 020509(R) (2010).
- <sup>54</sup>J. Jaroszynski, F. Hunte, L. Balicas, Y.-j. Jo, I. Raičević, A. Gurevich, D. C. Larbalestier, F. F. Balakirev, L. Fang, P. Cheng, Y. Jia, and H. H. Wen, *Phys. Rev. B* **78**, 174523 (2008).
- <sup>55</sup>S. J. Zhang, X. C. Wang, Q. Q. Liu, Y. X. Lv, X. H. Yu, Z. J. Lin, Y. S. Zhao, L. Wang, Y. Ding, H. K. Mao, and C. Q. Jin, *Europhys. Lett.* **88**, 47008 (2009).
- <sup>56</sup>H. Wadati, I. Elfimov, and G. A. Sawatzky, *Phys. Rev. Lett.* **105**, 157004 (2010).
- <sup>57</sup>T. Berlijn, C. H. Lin, W. Garber, and W. Ku, *Phys. Rev. Lett.* **108**, 207003 (2012).
- <sup>58</sup>K. Nakamura, R. Arita, and H. Ikeda, *Phys. Rev. B* **83**, 144512 (2011).
- <sup>59</sup>M. G. Kim, J. Lamsal, T. W. Heitmann, G. S. Tucker, D. K. Pratt, S. N. Khan, Y. B. Lee, A. Alam, A. Thaler, N. Ni, S. Ran, S. L. Bud'ko, K. J. Marty, M. D. Lumsden, P. C. Canfield, B. N. Harmon, D. D. Johnson, A. Kreyssig, R. J. McQueeney, and A. I. Goldman, *Phys. Rev. Lett.* **109**, 167003 (2012).